# Discrete approach to self-consistent *GW* calculations in an electron gas

Y. Dewulf, D. Van Neck, and M. Waroquier

*Laboratory for Theoretical Physics, University of Ghent Proeftuinstraat 86, B-9000 Gent, Belgium*
(Received 4 February 2005; published 30 June 2005)

Recent debate considering the importance of combining the *GW* approach to the electron gas with vertex corrections urges a calculation that can deal with both concepts in a self-consistent way. A major difficulty is the complicated energy dependence of the electron spectral function. We therefore propose an approximation for the Green's function that may be very useful for tackling a more complete treatment of the electron gas problem. The key concept in this approach is the representation of the Green's function by a limited number of carefully chosen poles. In this paper we present results for self-consistent *GW* calculation and find that they compare quite well to other self-consistent approaches. This legitimizes the use of this scheme as a practical tool for more involved calculations.

## I. INTRODUCTION

Although an overt simplification, the homogeneous electron gas or jellium can be linked to realistic electron systems such as metals and semiconductors. Furthermore, the correlation energy obtained for the electron gas at different densities serves as valuable input in density functional theory (DFT). In recent years there has been a growing interest to go beyond conventional DFT by using concepts from many-body perturbation theory. For applications in inhomogenuous systems this would require, apart from the correlation energy, more detailed knowledge of the electron self-energy in the electron gas.

Within the framework of many-body perturbation theory the *GW* approach[1,2] is the most common approach for studying correlations beyond the mean field in the electron gas. In the *GW* scheme the electron self-energy has a Fock-like structure where the propagator $G$ is coupled to a dynamically screened interaction $W$ which replaces the bare Coulomb interaction. This effective interaction sums the infinite set of ring diagrams. In its simplest incarnation this leads to the $G_0W_0$ approach, where the free electron propagator $G_0$ appears in the self-energy and is also used for the effective interaction $W_0$ calculated through the random phase approximation (RPA).

As with all schemes rooted in Green's function theory, self-consistency is an important issue. Already in 1962 the concept of self-consistency was linked to a number of conservation laws such as the conservation of particle number and energy when external perturbations are applied.[3] Within the *GW* scheme self-consistency requires that the free polarization be replaced by a polarization in which the particle and hole lines are dressed by the medium. This leads to an effective interaction $W$ different from $W_0$ associated with the analytical Lindhard function. The resulting set of coupled equations is solved by an iterative procedure.

Altough the need for self-consistency is well accepted in some fields of physics like nuclear matter calculations,[4] its necessity is much more under debate when looking at the electron gas problem. The reason for this reluctance is the fact that fully self-consistent *GW* calculations, when compared to $G_0W_0$, lead to inferior results for a number of important quantities such as the band gap and the position of the plasmaron satellite peaks. On the other hand, correlation energies calculated within the *GW* approach are in very good agreement with Monte Carlo results for densities $r_s > 1$.[5,6] It is common belief that vertex corrections will remedy the shortcomings of the standard self-consistent *GW* and will, e.g., reduce the *GW* band gap.

Some attempts have been made to incorporate vertex corrections, but with contradictory results depending on the amount of self-consistency and the type of vertex corrections retained in the calculations. A calculation that takes into account selected higher-order diagrams to the self-energy[7] finds a restoration of the $G_0W_0$ bandwidth. In some recent papers[8,9] an enhancement is found comparable to the self-consistent *GW* result, and it is suggested that the experimental sodium photoemission data, to which the electron gas results are usually compared, have been misinterpreted. While this suggestion has been criticized,[10] the results in Refs. 8 and 9 seem to be consistent with variational Monte Carlo results for the sodium lattice.[11] Recently, the problem was studied[12] in a (Hubbard) lattice model by combining extended dynamical mean-field theory (where cancellation of vertex corrections and self-energy insertions occurs locally to infinite order) with a $G_0W_0$ treatment of nonlocal correlations.

It seems clear that the final word on this issue should await a fully self-consistent calculation including most of the vertex corrections beyond the standard *GW* approach. It is, however, very difficult to go beyond the *GW* approach while retaining the full energy dependence of all involved quantities. A commonly used technique[13,14] is switching to ($T=0$)) imaginary-time Green's functions, thereby replacing rapid variations in the real-energy domain with decaying exponentials, rendering much smoother integrands for energy integrations. To obtain spectral information one needs to go back to the real-energy domain using analytical continuations, and while this seems to be under control at the *GW* level, there seems to be much less experience with extensions of *GW*, except when a simplified energy dependence for the vertex function is introduced.[8] A simple but reliable approximation for the Green's function may therefore be indispensable for the purpose of going beyond *GW*.

Motivated by successful applications in nuclear matter calculations,[4,15] we propose a scheme in which the continu-

ous Green's function is approximated by a restricted number of discrete poles. The location of the poles and the corresponding residues are chosen judiciously so that the approximated Green's function exhibits the same physical features as the continuous one during each iteration.

Section II starts with a brief summary of the self-consistent $GW$ formalism applied to the electron gas, followed by a discussion on the two different discretization schemes used in this paper. Section III presents the numerical results and a comparison to both the $G_0W_0$ and other self-consistent calculations. In addition to a detailed discussion for the $r_s=4$ case, also the density dependence of some key quantities is presented. The final section is reserved for some concluding remarks as well as some hints on how to go beyond the standard $GW$ scheme by including additional correlations. Throughout this paper atomic units are used.

## II. FORMALISM

In this section we briefly recapitulate the aspects of Green's function theory relevant for $GW$ calculations. More details can be found in textbooks on this subject (see, e.g., Ref. 16). The translational invariance of the electron gas dictates the use of the plane-wave single-particle basis. In the unpolarized electron gas the one-particle Green's function is independent of spin and completely determined by the magnitude of the momentum $p=|\vec{p}|$ and the energy $\omega$ of the particle.

Using Lehmann's representation, the Green's function can be written in terms of the removal and addition spectral functions $S_-$ and $S_+$,

$$G(p,\omega) = \int_{-\infty}^{\epsilon_F} d\omega' \frac{S_-(p,\omega')}{\omega - \omega' - i\eta} + \int_{\epsilon_F}^{+\infty} d\omega' \frac{S_+(p,\omega')}{\omega - \omega' + i\eta},$$ (1)

where $\epsilon_F$ is the Fermi energy of the system. For free electrons the spectral functions defining the noninteracting propagator $G^{(0)}(p,\omega)$ reduce to a single $\delta$ peak located at the kinetic energy $\omega=p^2/2$ of the electron. The free Fermi energy is $\epsilon_F=p_F^2/2$, where $p_F$ is the Fermi momentum corresponding to an electron density $\rho=2p_F^3/(3\pi^2)$.

When the electron-electron interactions are included the spectral functions will be of a more complicated nature and besides the reduced quasiparticle peak can have several satellite peaks added to a broad background distribution. The medium modifies the spectral functions through the (irreducible) self-energy $\Sigma(p,\omega)$. The specific shape of the spectral functions is then governed by Dyson's equation

$$G(p,\omega) = G^{(0)}(p,\omega) + G^{(0)}(p,\omega)\Sigma(p,\omega)G(p,\omega),$$ (2)

which can be transformed into the following expression for the spectral functions:

$$S_\pm(p,\omega) = \frac{1}{\pi} \frac{|\text{Im}\,\Sigma(p,\omega)|}{[\omega - p^2/2m - \text{Re}\,\Sigma(p,\omega)]^2 + [\text{Im}\,\Sigma(p,\omega)]^2}.$$ (3)

The self-energy can be expanded in an infinite series of diagrams containing only the Coulomb interaction and the

Green's function as building blocks. Alternatively, one can express the self-energy in terms of the exact two-particle Green's function $G_{II}$. Making suitable approximations for $G_{II}$ then allows us to sum infinite subsets of the original perturbation series which are most relevant for the system under study. In the $GW$ approach the self-energy only incorporates the subset of ring diagrams, providing an exact description in the high-density limit. The ring diagrams can be regrouped into a single quantity, the energy-dependent effective interaction $W$,

$$W(q,\omega) = v(q) + v(q)\Pi_0(q,\omega)W(q,\omega),$$ (4)

where $v(p)=4\pi/q^2$ is the Coulomb interaction and $\Pi_0$ is the dressed polarization propagator,

$$\Pi_0(q,\omega) = 2\int \frac{d^3q'}{(2\pi)^3} \int \frac{d\omega'}{2\pi i} G(q',\omega')G(|\vec{q}+\vec{q}'|,\omega+\omega').$$ (5)

In the numerical implementation, the imaginary part of $W$ is obtained from

$$\text{Im}\,W(q,\omega) = \frac{v^2(q)\text{Im}\,\Pi_0(q,\omega)}{[1 - v(q)\text{Re}\,\Pi_0(q,\omega)]^2 + v^2(q)\text{Im}\,\Pi_0(q,\omega)^2},$$ (6)

while the imaginary part of the $\Pi_0$ dressed polarization is calculated as a convolution of the spectral functions,

$$\text{Im}\,\Pi_0(q,\omega) = -2\pi \int \frac{d^3q'}{(2\pi)^3} \int_{-\infty}^{\epsilon_F} d\omega'$$
$$\times S_+(|\vec{q}+\vec{q}'|,\omega+\omega')S_-(q,\omega'),$$ (7)

for $\omega>0$. For negative energies one can exploit the symmetry relation $\Pi_0(q,\omega)=\Pi_0(q,-\omega)$. One should remark that $\Pi_0$ contains the energy dependence of the dressed spectral function. As a consequence $W$ differs from the commonly used approximation $W_0$ evaluated with the noninteracting $\Pi_0^{(0)}$, which is related to the Lindhard function.[16,17] The real part of $\Pi_0$ follows from a dispersion relation

$$\text{Re}\,\Pi_0(q,\omega) = \frac{1}{\pi}\mathcal{P}\int_{-\infty}^0 d\omega' \frac{\text{Im}\,\Pi_0(q,\omega')}{\omega - \omega'}$$
$$- \frac{1}{\pi}\mathcal{P}\int_0^{+\infty} d\omega' \frac{\text{Im}\,\Pi_0(q,\omega')}{\omega - \omega'}.$$

The real part of $W$ obeys a similar dispersion relation.

From the definition, Eq. (6), of the effective interaction, one sees the possible appearance of a discrete pole at a solution of

$$\Omega_{pl}(q) = 1 - v(q)\text{Re}\,\Pi_0(q,\Omega_{pl}(q)),$$ (8)

for which $\text{Im}\,\Pi_0(q,\Omega_{pl}(q))=0$. In the case of $W_0$ this is the well-known plasmon branch that leads to the classical plasmon frequency $\Omega_0=\sqrt{4\pi\rho}$ for $q\to0$. At a certain critical momentum, this plasmon pole disappears in the continuum. When retaining the complete energy dependence of the spectral function in a self-consistent $GW$ calculation, the imagi-

nary part of $\Pi_0$ will be nonzero for all energies and there will be no plasmon poles. As will be illustrated below, within our discrete approach the imaginary part of $\Pi_0$ still has plasmon poles in a limited momentum range. Because of the possibility of the plasmon pole the energy-dependent part of the self-energy contains in general two contributions. The first contribution arises from the continuum,

$$
\operatorname{Im}\Sigma^C(p,\omega) = -\int \frac{d^3q}{(2\pi)^3}\int_{-\infty}^{\epsilon_F}d\Omega\,\operatorname{Im}W(q,\omega-\Omega')
$$
$$
\times\,\theta(\Omega-\omega)S_-(|\vec{p}+\vec{q}|,\Omega)
$$
$$
+\int \frac{d^3q}{(2\pi)^3}\int_{\epsilon_F}^{+\infty}d\Omega\,\operatorname{Im}W(q,\omega-\Omega)
$$
$$
\times\,\theta(\Omega-\omega)S_+(|\vec{p}+\vec{q}|,\Omega), \tag{9}
$$

with $\theta(x)$ the Heaviside step function. It is easily checked that the first (second) integral only contributes for $\omega<\epsilon_F$ ($\omega>\epsilon_F$).

The second contribution arises from the plasmon pole (if present) in the effective interaction,

$$
\operatorname{Im}\Sigma^P(p,\omega) = -\int \frac{d^3q}{(2\pi)^3}\left.\frac{\partial\Pi_0(q,\Omega)}{\partial\Omega}\right|_{\Omega=-\Omega_{pl}(q)}
$$
$$
\times\,S_-(|\vec{p}+\vec{q}|,\omega+\Omega_{pl}(q))
$$
$$
+\int \frac{d^3q}{(2\pi)^3}\left.\frac{\partial\Pi_0(q,\Omega)}{\partial\Omega}\right|_{\Omega=+\Omega_{pl}(q)}
$$
$$
\times\,S_+(|\vec{p}+\vec{q}|,\omega-\Omega_{pl}(q)). \tag{10}
$$

The corresponding real part of the self-energy is calculated from a dispersion integral,

$$
\operatorname{Re}\Sigma^{C,P}(p,\omega) = \frac{1}{\pi}\mathcal{P}\int_{-\infty}^{\epsilon_F}d\omega'\frac{\operatorname{Im}\Sigma^{C,P}(p,\omega')}{\omega-\omega'}
$$
$$
-\frac{1}{\pi}\mathcal{P}\int_{\epsilon_F}^{+\infty}d\omega'\frac{\operatorname{Im}\Sigma^{C,P}(p,\omega')}{\omega-\omega'}. \tag{11}
$$

The total self-energy is the sum of both contributions and of the Hartree-Fock-like contribution $\Sigma^{\mathrm{HF}}$, which is real and independent of energy,

$$
\Sigma(p,\omega) = \Sigma^{\mathrm{HF}}(p)+\Sigma^P(p,\omega)+\Sigma^C(p,\omega), \tag{12}
$$

where

$$
\Sigma^{\mathrm{HF}}(p) = -\int \frac{d^3q}{(2\pi)^3}\int_{-\infty}^{\epsilon_F}d\omega\,v(q)S_-(|\vec{p}+\vec{q}|,\omega)
$$
$$
= -\int \frac{d^3q}{(2\pi)^3}\frac{1}{q^2}n(|\vec{p}+\vec{q}|). \tag{13}
$$

Note that $\Sigma^{\mathrm{HF}}(p)$ depends on the correlated momentum distribution,

$$
n(p) = \int_{-\infty}^{\epsilon_F}S_-(p,\omega)d\omega. \tag{14}
$$

At this point the self-consistency loop is closed, as both the polarization propagator (7) and the self-energy (9), (10), and (13) depend on the spectral function, which is itself calculated from the self-energy according to Eq. (3). This coupled set of integral equations is solved by iteration. One starts from a first guess for the spectral function, usually the single-peak free spectral function, and then proceeds with calculating the dressed polarization $\Pi_0$, the screened interaction $W$, and the self-energy $\Sigma$. From the Dyson equation, one obtains a new estimate for the spectral function. This new estimate is used to repeat the calculation, until convergence is reached.

The energy dependence of the dressed spectral function is rather complicated, including several sharp peaks and a broad background distribution. Accurate evaluation of the polarization and self-energy is not straightforward. Certainly if one wants to go beyond the *GW* scheme and include vertex corrections, there is a strong need for a reliable approximation to the spectral function. Such an approximation should be sufficiently simple in order to speed up the calculations, while at the same time should contain the relevant physics. Motivated by previous work in other many-body systems such as electrons in atoms,[18] atomic nuclei,[19] nuclear matter,[4] and neutron matter[20] we want to explore an approximation to the Green's function in terms of a small number of discrete poles. An approach somewhat similar in spirit can be found in Ref. 21, where the (removal) spectral function is approximated by a sequence of $\delta$ peaks separated by multiples of the plasmon energy. This form is inspired by the schematic electron-plasmon model and was able to generate correct total energies through the Migdal-Galitskii sum rule. However, in contrast to the present work no self-consistency scheme was attempted.

In this paper we will limit ourselves to a calculation with three poles. The idea is that one pole describes the position and strength of the quasi particle peak, while the others represent the continuous background distribution and additional peaks in the removal ($\omega<\epsilon_F$) and addition ($\omega>\epsilon_F$) domain of the spectral function. Such a "minimal" propagator can be written as

$$
G(p,\omega) = \frac{z_-(p)}{\omega-E_-(p)-i\eta}+\frac{z_c(p)\,\theta(p_F-p)}{\omega-E_c(p)-i\eta}+\frac{z_c(p)\,\theta(p-p_F)}{\omega-E_c(p)+i\eta}
$$
$$
+\frac{z_+(p)}{\omega-E_+(p)+i\eta}. \tag{15}
$$

It is clear from Eq. (15) that the removal spectral function is approximated by two poles for hole states ($p<P_F$), but by just one pole for a particle states ($p>p_F$). The inverse holds for the addition spectral function. The location of the three poles $E_i$ (where $i=-,c,+$), and the value of the corresponding residues $z_i$ must be chosen in such a way that they constitute an optimal representation of the exact spectral functions $S_\pm(p,\omega)$. As there is a certain freedom associated with this choice, we briefly summarize the conditions that should be satisfied by any physical discretization scheme. First of all, the position of the central pole must be chosen so as to coincide with the quasiparticle peak in the spectral function. This means that its location is fixed at the on-shell energy

$$\epsilon_{qp}(p) = \frac{p^2}{2} + \mathrm{Re}\Sigma(p, \omega_{qp}(p)). \qquad (16)$$

Second we want to reproduce the correct zeroth- and first-order moments of the spectral function, defined as ($k=0$, 1)

$$m_-^{(k)}(p) = \int_{-\infty}^{\epsilon_F} \omega^k S_-(p, \omega) d\omega, \qquad (17)$$

$$m_+^{(k)}(p) = \int_{\epsilon_F}^{+\infty} \omega^k S_+(p, \omega) d\omega. \qquad (18)$$

The characterization of the spectral function in terms of its lowest-order energy-weighted moments has been examined in Ref. 22. Here we insist on reproducing the moments separately for the removal and addition domain. By doing so, one reproduces the correct occupation probability, $n(p) = m_-^{(0)}(p)$, as well as the binding energy as it would be obtained from the exact spectral function through the Migdal-Galitskii sum rule,

$$E/A = \frac{1}{\rho} \int_{-\infty}^{\epsilon_F} d\omega \int \frac{d^3p}{(2\pi)^3} \left( \frac{p^2}{2} + \omega \right) S_-(p, \omega)$$

$$= \frac{1}{\rho} \int \frac{d^3p}{(2\pi)^3} \left( \frac{p^2}{2} m_-^{(0)}(p) + m_-^{(1)}(p) \right). \qquad (19)$$

The one remaining degree of freedom is the assignment of the strength of the central pole. The conventional expression for the quasiparticle strength,

$$z_{qp} = \left( 1 - \left. \frac{\partial \mathrm{Re}\Sigma(p, \omega)}{\partial \omega} \right|_{\omega = \epsilon_{qp}(p),} \right)^{-1}, \qquad (20)$$

derived by expanding the spectral function around the quasiparticle energy, is in principle only valid near $p_F$ and may lead to unreasonable results ($z_{qp} > 1$) for $p \gg p_F$.

Therefore we investigated some alternative ways of separating the quasiparticle peak from the background. In this paper we will present results for two particular schemes, which will be labeled scheme $A$ and scheme $B$ throughout the paper. Scheme $A$ starts from the somewhat simplified assumption that for all momentum states the fraction of quasiparticle strength to background strength remains fixed, equaling the fraction at the Fermi momentum. This means that for hole states ($p < p_F$) the residues and energies are obtained from the fraction $f_- = z_c(p_F)/[z_-(p_F) + z_c(p_F)]$ and

$$z_-(p) = [1 - f_-] m_-^{(0)}(p), \quad z_c(p) = f_- m_-^{(0)}(p), \quad z_+(p) = m_+^{(0)}(p), \qquad (21)$$

$$E_-(p) = m_-^{(1)}(p) - \epsilon_{qp}(p) z_c(p), \qquad (22)$$

$$E_c(p) = \epsilon_{qp}(p), \quad E_+(p) = m_+^{(1)}(p)/m_+^{(0)}(p), $$

whereas for particle states ($p > p_F$) one has $f_+ = z_c(p_F)/[z_+(p_F) + z_c(p_F)]$ and

$$z_-(p) = m_-^{(0)}(p), \quad z_c(p) = f_+ m_+^{(0)}(p), \quad z_+(p) = [1 - f_+] m_+^{(0)}(p), \qquad (23)$$

$$E_-(p) = m_-^{(1)}(p)/m_-^{(0)}(p), \quad E_c(p) = \epsilon_{qp}(p), \quad E_+(p) = m_+^{(1)}(p) - \epsilon_{qp}(p) z_c(p). \qquad (24)$$

It should be noted that $z_-(p_F)$, $z_c(p_F)$, and $z_+(p_F)$ are unambiguously defined, since the quasiparticle pole for the Fermi momentum has zero width and is, by definition, located at the Fermi energy. The residues $z_-(p_F)$ and $z_+(p_F)$ can be determined by integrating the smooth hole and particle spectral function, while $z_c(p_F)$ corresponds to the missing strength in the sum rule:

$$z_c(p_F) = 1 - z_-(p_F) - z_+(p_F). \qquad (25)$$

Especially for large momenta scheme $A$ is an oversimplification, as the strength $z_c(p)$ associated with the quasiparticle pole should approach unity in this limit. However, for $p \rightarrow \infty$ the energy difference between two forward poles, $E_c(p)$ and $E_+(p)$, becomes negligible, so that they can be regarded as one pole with a strength equal to unity.

Scheme $B$ fixes the value of $z_c(p)$ by requiring the additional reproduction of the inverse central moment

$$m_-^{(-1)}(p) = \int_{-\infty}^{\epsilon_F} (\omega - \epsilon_F)^{-1} S_-(p, \omega) d\omega \qquad (26)$$

for hole states and likewise $m_+^{(-1)}(p)$ for particle states. The inverse moment gives more weight to the low-energy region of the spectral function and less to the high-energy tails. Several other schemes have been investigated, including hybrid schemes which use $z_{qp}$ [Eq. (20)] as $z_c$ for hole states and either scheme $A$ or $B$ for particle states. All of the schemes gave similar results, so the presented results for scheme $A$ and scheme $B$ give an indication of the error originating from the choice of discretization scheme.

The positions $E_i(p)$ and strengths $z_i(p)$ of the propagator poles obtained after convergence for both schemes $A$ and $B$ are illustrated in Fig. 1. The most pronounced differences are found for the $z_i$. In scheme $A$, the strength of the forward pole $z_+(p)$ is always proportional to $1 - n(p)$ for $p > p_F$, hence the smooth behavior. Scheme $B$ shows a more complicated momentum dependence and, for large momenta, locates all strength in the central (quasiparticle) pole. This difference in the partition of strength is also reflected in the corresponding energies. Surprisingly, it turns out that two features are rather independent of the specific scheme. First, the location of the central peak is not affected by the choice of discretization scheme. This is not at all trivial, as the spectra shown in Fig. 1 are converged spectra and in each iteration the on-shell energy and the real part of the self-energy depend on the location and strength of the other poles. Since the central pole is connected to the quasiparticle properties—e.g., the Fermi energy and the bandwidth—it is clear that these will be hardly different in both schemes. Second, one sees that the energy $E_-$ of the backward pole is different in both schemes for $p < p_F$, but has the same behavior, $E_- \sim -p^2/2m$, for momenta $p > p_F$. This is the pole responsible for the high-momentum components in the electronic many-body wave function.
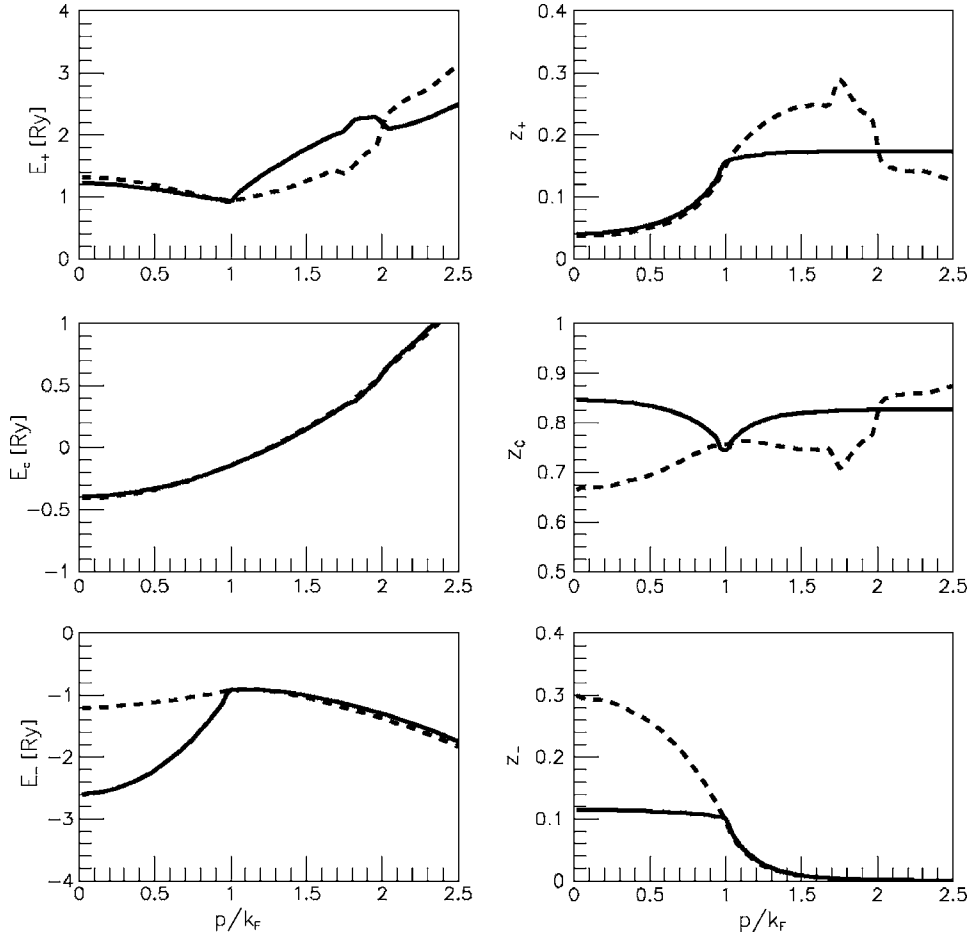
FIG. 1. The location and strength of the poles for $r_s = 4$ in the three-pole scheme *A* (solid line) and scheme *B* (dashed line) after convergence.

As a final remark we note that, when determining the moments of the spectral function, it is always possible to avoid an integration over the quasiparticle peak (which may be very sharp for states close to the Fermi momentum) by taking advantage of the sum rules

$$m_+^{(0)}(p) + m_-^{(0)}(p) = 1, \qquad (27)$$

$$m_+^{(1)}(p) + m_-^{(1)}(p) = \epsilon^{\mathrm{HF}}(p), \qquad (28)$$

$$m_+^{(-1)}(p) + m_-^{(-1)}(p) = 1/[\epsilon^{\mathrm{HF}}(p) - \epsilon_F - M^{(-1)}(p)], \quad (29)$$

where $\epsilon^{\mathrm{HF}}(p) = p^2/2 + \Sigma^{\mathrm{HF}}(p)$ is the Hartree-Fock single-particle energy and the inverse central moment of the self-energy strength is defined as

$$M^{(-1)}(p) = \frac{1}{\pi} \int_{-\infty}^{\infty} d\omega \frac{|\mathrm{Im}\,\Sigma(p,\omega)|}{\omega - \epsilon_F}. \qquad (30)$$

### III. RESULTS

As the present approximations are proposed as an alternative starting point for more involved many-body calculations, it is instructive to compare the discrete approach with the $G_0 W_0$ approach and with other self-consistency implementations.[5] In the remainder of this paper all energies are given in rydbergs. Except when stated otherwise, a solid

line refers to results obtained with discretization scheme *A*, a dashed line to scheme *B*, and a dotted line refers to the first iteration, which corresponds to a $G_0 W_0$ calculation using the free Green's function $G_0$ as input.

In the first part of this section, we will show how the presence of two additional discrete poles modifies the screened interaction, the self-energy, and the spectral function. When starting from a given approximation for the Green's function, the first quantity that is calculated in the procedure sketched above is the imaginary part of the polarization $\Pi_0$. Using a three-pole spectrum as input, the imaginary part is calculated from

$$\mathrm{Im}\,\Pi_0(p,\omega) = -2\pi \sum_{i=c,+} \sum_{j=-,c} \int \frac{d^3 q}{(2\pi)^3} z_i^>(|\vec{p} + \vec{q}|) z_j^<(q)$$

$$\times \delta(\omega - E_i(|\vec{p} + \vec{q}|) + E_j(q)), \qquad (31)$$

where the notation

$$z_i^<(p) = [1 - \delta_{i,c}\theta(p - p_F)]z_i(p), \qquad (32)$$

$$z_i^>(p) = [1 - \delta_{i,c}\theta(p_F - p)]z_i(p)$$

has been used.

In Fig. 2 we compare the free $\mathrm{Im}\,\Pi_0^{(0)}$ to the self-consistent *GW* result for $\mathrm{Im}\,\Pi_0$ after convergence within both discretization schemes. The low-energy domain shown in the left panel is the only energy region that contributes in
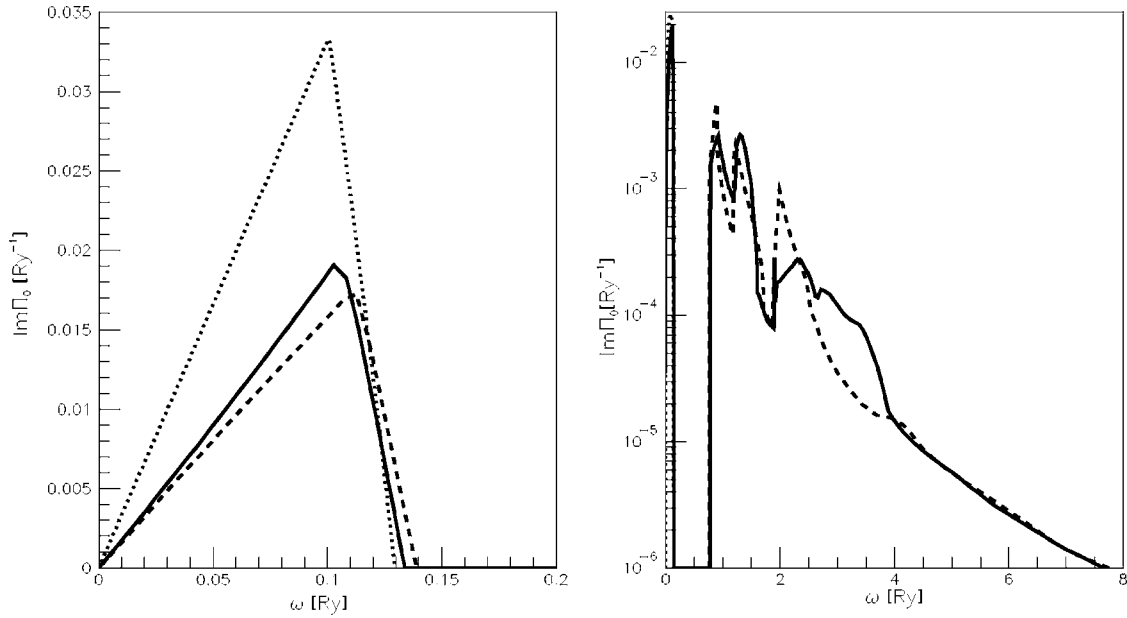
FIG. 2. The imaginary part of the polarization for $r_s=4$ and $p=0.02p_F$ obtained within scheme $A$ (solid line) and scheme $B$ (dashed line) after convergence. Also shown is the result after the first iteration (dotted line), which equals the Lindhard function.

the first-iteration (dotted line). Comparing the first iteration result with the self-consistent result we note that Im $\Pi_0$ has a reduction of strength in this region, while the structure is somewhat broadened. The first observation follows from the reduction of quasiparticle strength, the second one from the difference in the quasiparticle spectrum. In the right panel of Fig. 2 a more extended energy domain is shown, which includes the high-energy tails in the self-consistent result. While the detailed shape of the distribution depends on the used discretization scheme, the threshold energy and the

high-energy tail are rather independent of this choice. The different peaks in this distribution are related to different combinations of discrete poles, the structure at low energy corresponding to the $(c,c)$ combination, while the broad distribution has contributions of $(c,+)$, $(-,c)$, and $(-,+)$ combinations. In contrast to Ref. 5, a gap in the Im $\Pi_0$ distribution persists due to the discrete nature of the present approach. This gap disappears for momenta above $0.8p_F$ (for $r_s=4$) and leads to collective plasmon poles in $W$ below the threshold energy.
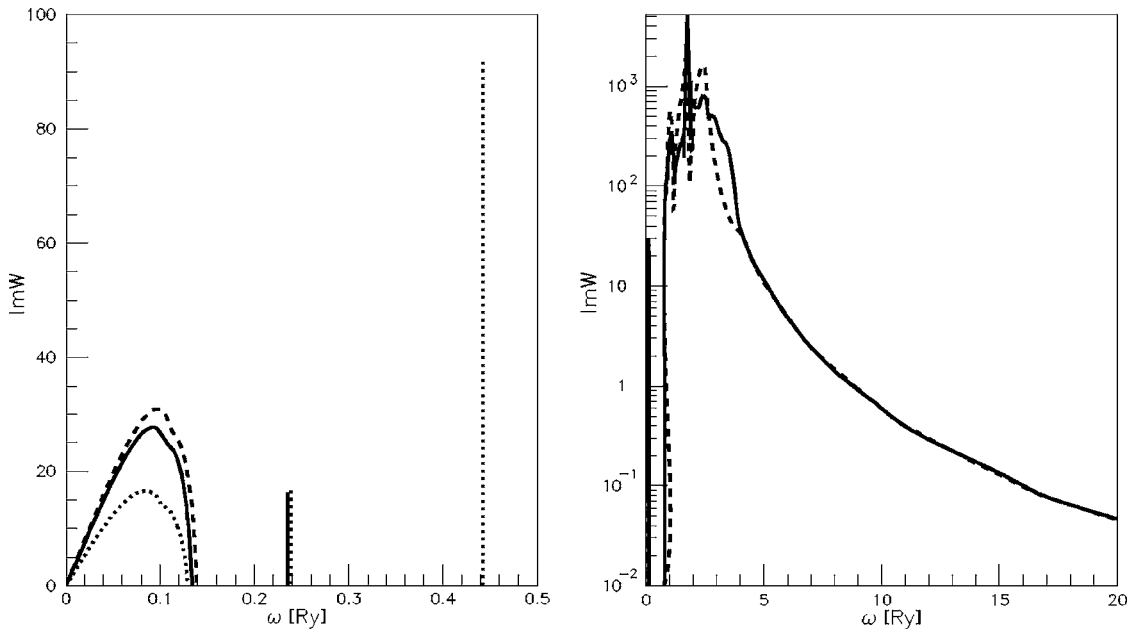


FIG. 3. The imaginary part of the screened interaction $W$ for $r_s=4$ and for $p=0.02p_F$ after the first iteration (dotted line) and after convergence for scheme $A$ (solid line) and scheme $B$ (dashed line). The vertical lines in the left panel indicate the positions of the $\delta$-peak contributions of the plasmon poles. Their height is proportional to $[\partial\Pi_0(q,\omega)/\partial\omega]^{-1}$.
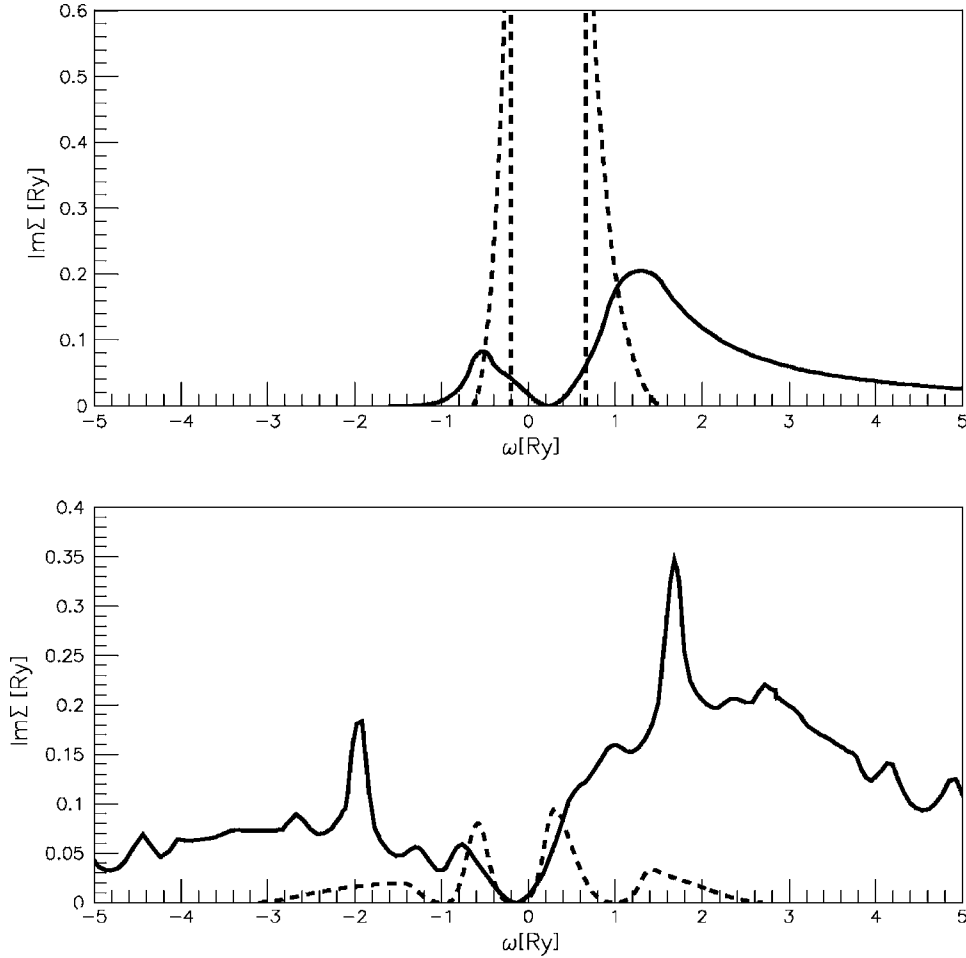
FIG. 4. The imaginary part of the self-energy for $r_s=4$ and $p=p_F$, after the first iteration (upper plot) and after convergence for scheme $A$ (lower plot). The solid line refers to the continuum contribution of Eq. (33), while the dotted line refers to the plasmon contribution in Eq. (34).

The corresponding imaginary part of the screened interaction $W$ for $q=0.02p_F$ is displayed in Fig. 3. In the low-energy region (left panel) we note that, compared to $W_0$, the quasiparticle distribution is enhanced because of the smaller value of the real part of the dielectric function $\epsilon(q,\omega)=1-v(q)\mathrm{Re}\,\Pi_0(q,\omega)$ for these energies. Also indicated (see caption) in the left panel is the position and strength of the plasmon poles. It is clear that within a self-consistent discrete pole approach there still are plasmon pole contributions to the self-energy, but their strength is seriously reduced compared to $W_0$. Unsurprisingly, the self-consistent results exhibit a broad distribution at high energies, shown in the right panel.

From the screened interaction and the discrete spectra we can calculate the continuum contribution to the imaginary part of the self-energy,

$$\mathrm{Im}\,\Sigma^C(p,\omega) = -\sum_{i=c,+} \int \frac{d^3q}{(2\pi)^3} \mathrm{Im}\,W(q,\omega - E_i(|\vec{p}+\vec{q}|))$$

$$\times z_i^>(|\vec{p}+\vec{q}|) \quad \text{if } \omega > \epsilon_F,$$

$$\mathrm{Im}\,\Sigma^C(p,\omega) = \sum_{i=-,c} \int \frac{d^3q}{(2\pi)^3} \mathrm{Im}\,W(q,\omega - E_i(|\vec{p}+\vec{q}|))$$

$$\times z_i^<(|\vec{p}+\vec{q}|) \quad \text{if } \omega > \epsilon_F, \tag{33}$$

as well as the plasmon contribution

$$\mathrm{Im}\,\Sigma^P(p,\omega) = -\sum_{i=-,c} \int \frac{d^3q}{(2\pi)^3} \left.\frac{\partial\Pi_0(q,\Omega)}{\partial\Omega}\right|_{\Omega=-\Omega_{pl}(q)}$$

$$\times z_i^<(|\vec{p}+\vec{q}|)\delta(\omega + \Omega_{pl}(q) - E_i(|\vec{p}+\vec{q}|))$$

$$+ \sum_{i=c,+} \int \frac{d^3q}{(2\pi)^3} \left.\frac{\partial\Pi_0(q,\Omega)}{\partial\Omega}\right|_{\Omega=+\Omega_{pl}(q)}$$

$$\times z_i^>(|\vec{p}+\vec{q}|)\delta(\omega - \Omega_{pl}(q) - E_i(|\vec{p}+\vec{q}|)). \tag{34}$$

Figure 4 displays these quantities for $p=p_F$ The upper panel refers to the first iteration, the lower panel to the self-consistent calculation using scheme $A$. The most striking difference is the enhancement and broadening of the continuum contribution in the removal domain. In a self-consistent calculation this distribution extends to $\omega \to -\infty$, while in the first iteration ($G_0W_0$) it has a minimum energy. Also the continuum distribution at positive energies is enhanced. The plasmon distribution broadens and has additional structure originating from the discrete nature of the spectral function. The relative importance of the plasmon constribution is seriously reduced, an effect that is the counterpart of the complete absence of plasmon contributions in a continuous approach. While the detailed structure of the self-energy obtained using scheme $B$ is slightly different, the same qualitive conclusions apply.
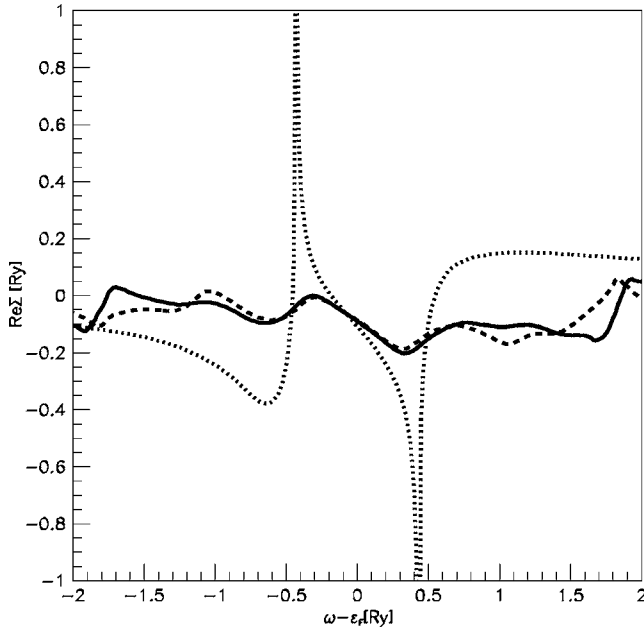
FIG. 5. The real part of the self-energy (excluding the Hartree-Fock contribution) for $r_s=4$ and $p=p_F$, after the first iteration (dotted line) and after convergence for scheme *A* (solid line) and scheme *B* (dashed line).

The real part of the self-energy as calculated from the dispersion relation (11) is shown in Fig. 5 for $p=p_F$. The sharp peaks near $\epsilon_F$ which dominate in the $(G_0W_0)$ first iteration disappear in the self-consistent calculation. As with the imaginary part, the additional peaks and valleys are a result of the discrete pole approximation, and are smoothed out in a continuous treatment.[5] While the detailed structure depends on the discretization scheme, the overall behavior is again rather independent of the specific scheme. Close to the on-shell energies, e.g., both self-consistent calculations have a smaller slope than the $G_0W_0$ self-energy. This leads to an enhanced value of the quasiparticle strength, in agreement with the known observation[5,7] that self-consistency in $GW$ causes a redistribution of single-particle strength in favor of the quasiparticle peak. The density dependence of this enhancement will be shown in Fig. 10.

Figure 6 shows the imaginary part of the self-energy at the on-shell energy. This quantity corresponds to the width of the quasiparticle excitation or to the inverse of its lifetime. The first iteration indicates very short lifetimes for quasiparticles with momenta above $2p_F$. This can be explained by inelastic collisions of the quasiparticle with plasmons. The self-consistent calculations, in which the plasmon contribution to the self-energy is very much reduced (or absent), do not predict these short lifetimes.

An example of the resulting spectral functions is shown in Fig. 7 for $p=0.25p_F$. The most remarkable feature is the reduction in strength and the broadening of the narrow $G_0W_0$ plasmaron satellite in the removal domain. The position of the plasmaron is shifted towards the quasiparticle peak. In the continuous $GW$ results of von Barth and Holm[5] the satellite peak is absent for all momenta, which again indicates that in the present discrete approach the contribution of the
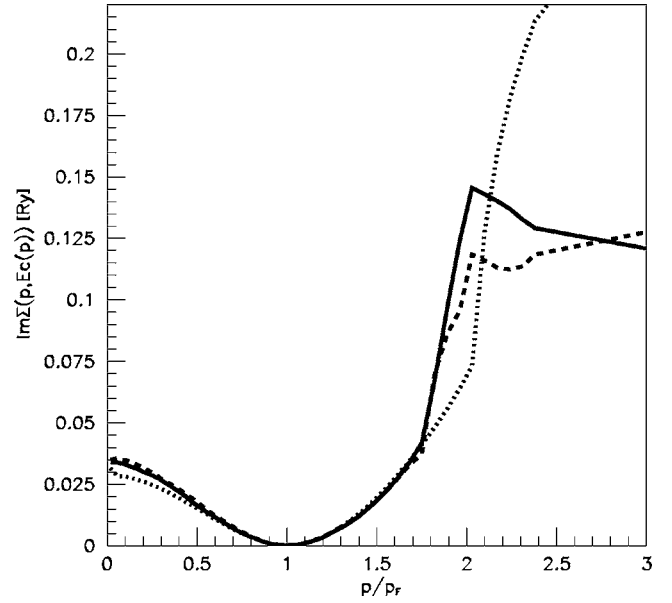


FIG. 6. The inverse lifetime of the quasiparticle excitation for $r_s=4$, after the first iteration (dotted line) and after convergence for scheme *A* (solid line) and scheme *B* (dashed line).

plasmons is much reduced but still significant for low momenta. The location of the plasmaron satellite is independent of the choice of discretization scheme.

Integrating the hole spectral function (14) leads to the momentum distribution, which is displayed in Fig. 8. It is clear that the first iteration shows a larger depletion of the Fermi sea. Since the $GW$ approach is number conserving, the free density of the electron gas should be retrieved when integrating the self-consistent occupation probability over all
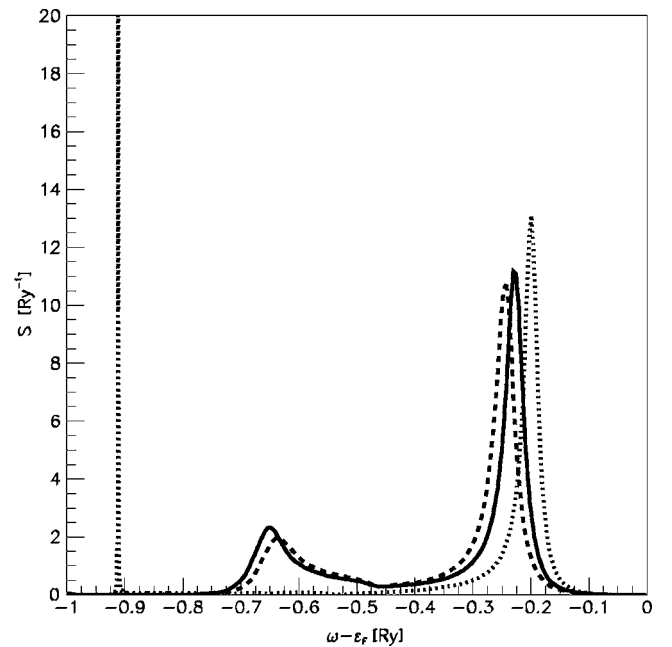


FIG. 7. The hole spectral function for $r_s=4$ and $p=0.25p_F$, after the first iteration (dotted line) and after convergence for scheme *A* (solid line), and scheme *B* (dashed line).
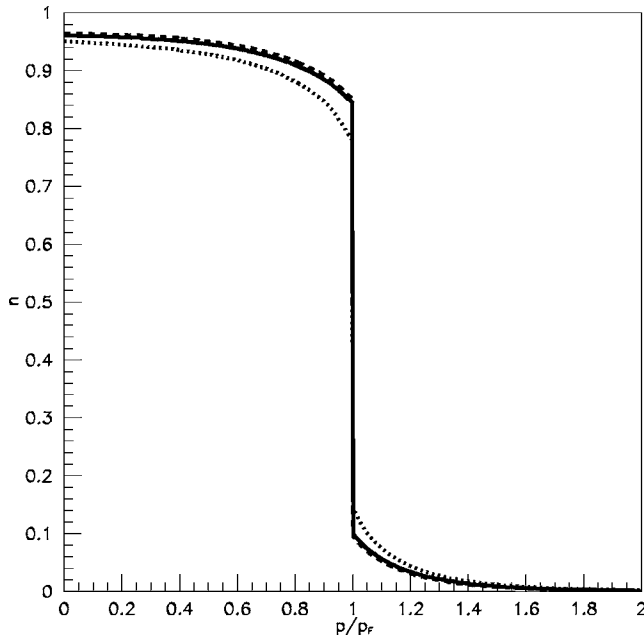
FIG. 8. The occupation probability for $r_s = 4$, after the first iteration (dotted line) and after convergence for scheme $A$ (solid line) and scheme $B$ (dashed line).

momenta. We checked that this property is satisfied to within our numerical accuracy.

The next figures show the density dependence of some key quantities and compare them to other available numbers. A crucial quantity is the bandwidth $\Delta$ which can be compared to the experimental value[23] for sodium, $\Delta \approx 2.6$ eV or $\Delta/(p_F^2/2) \approx 0.8$ for a density corresponding to $r_s \approx 4$. The



FIG. 10. The density dependence of the quasi particle strength after the first iteration (dotted line) and after convergence for scheme $A$ (solid line) and scheme $B$ (dashed line). The triangles and circles refer to the $GW_0$ and $GW$ results, respectively, taken from Ref. 5.

bandwidth is defined as the energy difference between the quasiparticle energies at zero and at the Fermi momentum, and results from a delicate balance between the static (Hartree-Fock-like) and the dynamic contributions to the
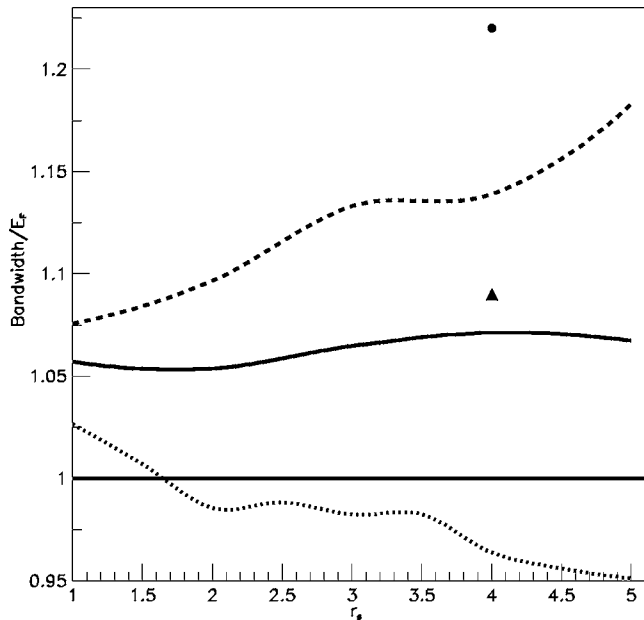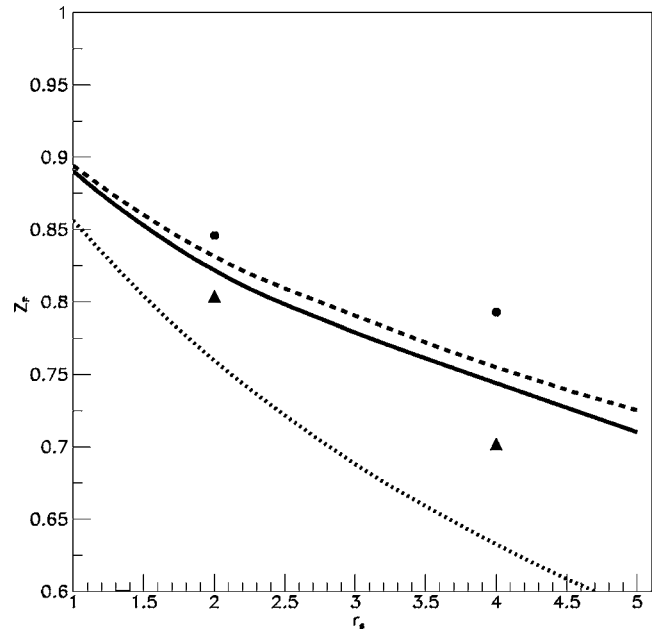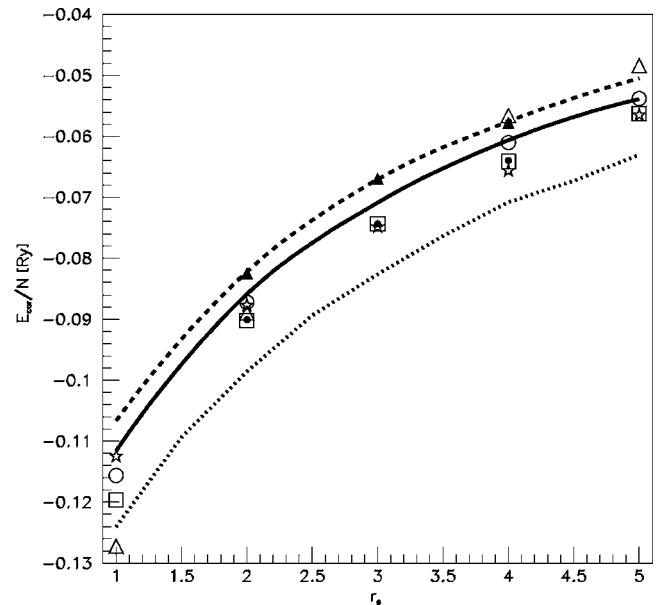


FIG. 9. The density dependence of the bandwidth (relative to the free Fermi energy) after the first iteration (dotted line) and after convergence for scheme $A$ (solid line) and scheme $B$ (dashed line). The triangle and circle correspond to the $GW_0$ and $GW$ results, respectively, taken from Ref. 5.



FIG. 11. The density dependence of the correlation energy after the first iteration (dotted line) and after convergence for scheme $A$ (solid line) and scheme $B$ (dashed line). The various symbols represent diffusion Monte Carlo results from Ref. 24 (squares) and from Ref. 25 (stars), $GW$ results from Ref. 6 (open circles) and from Ref. 5 (solid circles), and $GW_0$ results from Ref. 6 (open triangles) and from Ref. 5 (solid triangles).

self-energy. The bandwidth of the free electron spectrum is too large compared to the experimental value. The $G_0W_0$ approach leads to a reduction, which is, however, too small to reproduce the experimental value. Self-consistent $GW$ calculations worsen the situation as they enlarge the bandwidth to values that are up to 20% larger than the value for noninteracting electrons. The results of both discrete pole calculations are shown in Fig. 9, together with the first-iteration result. Also shown are the self-consistent $GW$ result and the partially self-consistent $GW_0$ result obtained with the continuous approach of Ref. 5. While we also treat the screened interaction self-consistently, the discrete approximation leads to bandwidths which are substantially smaller than those obtained in the continuous $GW$ approach. The result obtained with scheme $A$ even leads to a value below the partially self-consistent $GW_0$ result. A possible explanation may again be found in the fact that we still retain plasmons for low momenta, although they are considerably reduced in strength.

Figure 10 shows the quasiparticle strength at the Fermi momentum for both discretization schemes and the first iteration. We see that in all three calculations the correlations increase with decreasing density (increasing values of $r_s$). On the same plot the results of Ref. 5 are displayed. Also for this quantity we see that the discrete approximation leads to results that are in between the fully self-consistent and the partially self-consistent result of Ref. 5.

The correlation energy, defined as the total energy per particle relative to the HF ground-state energy, is shown in Fig. 11. Also displayed on this plot are diffusion Monte Carlo calculations by Ceperley and Alder,[24] and by Ortiz and Ballone,[25] as well as $GW$ and $GW_0$ results by Refs. 5 and 6. The present discrete approximations are clearly capable of reproducing (though somewhat overshooting in case of scheme $B$) the main effect in the energy shift from $G_0W_0$ to $GW$. In fact, as with all quantities discussed in this paper, it appears that a discrete approximation leads to values in between continuous $GW_0$ and $GW$ results.

## IV. CONCLUSION

In order to gain a more detailed understanding of the electronic self-energy in the homogeneous electron gas (and by extension in other electronic systems such as metals, semiconductors, atoms, and molecules), it will be necessary to go beyond $GW$ and incorporate both vertex corrections and the concept of self-consistency. At present we think it might be useful to consider solving the two-particle one-hole Fadeev equations[26] for the electron gas, as they treat the correlations between particles and holes in a fully symmetric way. It is doubtful whether the complete energy dependence of the spectral functions can be retained at this level of perturbation theory. In this paper we propose a discrete pole representation of the Green's function that greatly facilitates the self-consistent evaluation of all relevant quantities. To demonstrate the power of such a scheme we applied it to a self-consistent $GW$ calculation without any vertex corrections and concluded that the results were comparable to the ones obtained in a scheme using a continuous parameterization.

In contrast to continuous calculations, the discrete approach still retains plasmon contributions to the self-energy, leading to remnants of satellite peaks in the spectral functions. Due to this feature, it might actually be a favorable starting point to go beyond a standard $GW$ calculation.

Considering the rather large reduction in computational effort compared to continuous schemes, we think that such a discrete approximation can be a very useful tool for a further investigation of the much debated interplay between vertex-corrections and self-consistency.

[1] L. Hedin, Phys. Rev. **139**, A796 (1965).
[2] B. I. Lundqvist, Phys. Kondens. Mater. **6**, 193 (1967); B. I. Lundqvist and V. Samathiyakanit, Phys. Kondens. Mater. **9**, 231 (1969).
[3] G. Baym and L. P. Kadanoff, Phys. Rev. **124**, 287 (1961).
[4] Y. Dewulf, W. H. Dickhoff, D. Van Neck, E. R. Stoddard, and M. Waroquier, Phys. Rev. Lett. **90**, 152501 (2003).
[5] U. von Barth and B. Holm, Phys. Rev. B **54**, 8411 (1996); B. Holm and U. von Barth, *ibid.* **57**, 2108 (1998); B. Holm, Phys. Rev. Lett. **83**, 788 (1999).
[6] P. Garcia-Gonzalez and R. W. Godby, Phys. Rev. B **63**, 075112 (2001).
[7] E. L. Shirley, Phys. Rev. B **54**, 7758 (1996).
[8] Y. Takada, Phys. Rev. Lett. **87**, 226402 (2001).
[9] H. Yasuhara, S. Yoshinaga, and M. Higuchi, Phys. Rev. Lett. **83**, 3250 (1999).
[10] W. Ku, A. G. Eguiluz, and E. W. Plummer, Phys. Rev. Lett. **85**, 2410 (2000).
[11] R. Maezono, M. D. Towler, Y. Lee, and R. J. Needs, Phys. Rev. B **68**, 165103 (2003).
[12] P. Sun and G. Kotliar, Phys. Rev. Lett. **92**, 196402 (2004); Phys. Rev. B **66**, 085120 (2002).
[13] H. N. Rojas, R. W. Godby, and R. J. Needs, Phys. Rev. Lett. **74**, 1827 (1995).
[14] M. M. Rieger, L. Steinbeck, I. D. White, H. N. Rojas, and R. W. Godby, Comput. Phys. Commun. **117**, 211 (1999).
[15] Y. Dewulf, D. Van Neck, and M. Waroquier, Phys. Rev. C **65**, 054316 (2002).
[16] A. L. Fetter and J. D. Walecka *Quantum Theory of Many-particle Systems* (McGraw-Hill, New York, 1971).
[17] J. Lindhard, K. Dan. Vidensk. Selsk. Mat. Fys. Medd. **28** (1954).
[18] D. Van Neck, K. Peirs, and M. Waroquier, J. Chem. Phys. **115**, 15 (2001); K. Peirs, D. Van Neck, and M. Waroquier, *ibid.* **117**, 4095 (2002).

[19] Y. Dewulf, D. Van Neck, L. Van Daele, and M. Waroquier, Phys. Lett. B **396**, 1 (1997).

[20] A. E. L. Dieperink, Y. Dewulf, D. Van Neck, M. Waroquier, and V. Rodin, Phys. Rev. C **68**, 064307 (2003).

[21] B. Holm and F. Aryasetiawan, Phys. Rev. B **62**, 4858 (2000).

[22] M. Vogt, R. Zimmermann, and R. J. Needs, Phys. Rev. B **69**, 045113 (2004).

[23] E. Jensen and E. W. Plummer, Phys. Rev. Lett. **55**, 1912 (1985).

[24] D. M. Ceperley and B. J. Alder, Phys. Rev. Lett. **45**, 566 (1980); D. Ceperley, Phys. Rev. B **18**, 3126 (1978).

[25] G. Ortiz and P. Ballone, Phys. Rev. B **50**, 1391 (1994); G. Ortiz, M. Harris, and P. Ballone, Phys. Rev. Lett. **82**, 5317 (1999).

[26] C. Barbieri and W. H. Dickhoff, Phys. Rev. C **63**, 034313 (2001); **65**, 064313 (2002).